Metal-to-Metal Distance Modulated Au(I)/Ru(II) Cyclophanyl Complexes: Cooperative Effects in Photoredox Catalysis

Christoph Zippel,[a] Roumany Israil,[b] Lars Schüssler,[c] Zahid Hassan,[a] Erik K. Schneider,[d] Patrick Weis,[d] Martin Nieger,[e] Claudia Bizzarri,[a] Manfred M. Kappes,[d, f] Christoph Riehn,[b, g] Rolf Diller,[c] and Stefan Bräse*[a, h]

Abstract: The modular synthesis of Au(I)/Ru(II) decorated mono- and heterobimetallic complexes with π-conjugated [2.2]paracyclophane is described. [2.2]Paracyclophane serves as a rigid spacer which holds the metal centers in precise spatial orientations and allows metal-to-metal distance modulation. A broad set of architectural arrangements of pseudo -geminal, -ortho, -meta, and -para substitution patterns were employed. Metal-to-metal distance modulation of Au(I)/Ru(II) heterobimetallic complexes and the innate transannular π-communication of the cyclophanyl scaffold provides a promising platform for the investigations of structure-activity relationship and cooperative effects. The Au(I)/Ru(II) hetero-bimetallic cyclophanyl complexes are stable, easily accessible, and exhibit promising catalytic activity in the visible-light promoted arylative Meyer-Schuster rearrangement.

Introduction

Heterometallic complexes have received considerable attention due to their distinctive magnetic and optical properties and further their emerging synthetic applications in catalysis.[1] Installation of heterometallic moieties in one framework – each intended to serve a particular, independent purpose, can execute precise sequences of multiple reactions in a one-pot fashion. The activity of one metal is enhanced by the other and in combination, may reduce the activation barrier by cooperative effects.[2] Incorporating a second metal center into mono-nuclear organometallic complexes can lead to novel reactivity and enhanced selectivity compared to the reaction performed with a mixture of related monometallic complexes.[3] However, it remains a synthetic challenge to position heteronuclear metal centers with a well-defined electronic environment in a pre-defined orientation to one another to achieve cooperative effects. Among various contributing factors based on the nature of the metal, oxidation state, and coordination number, metal-to-metal (M–M) distance modulation has been a promising approach to identify and fine-tune cooperative effects in (hetero)bimetallic systems.[4] Especially the bridging ligand design is decisive to incorporate multiple metal centers in defined orientations and stands in the center from a perspective of application.[5] The choice of the coordination environment, ligand effects like flexibility, sterics, electronic parameters, and an appropriate spacer that allows for systematic variation of M–M distances are crucial contributing factors.[6] The presence of two or more metal centers with defined M–M distances can be achieved either by a conjugated or non-

[a]   C. Zippel, Dr. Z. Hassan, Dr. C. Bizzarri, Prof. Dr. S. Bräse
      Institute of Organic Chemistry (IOC)
      Karlsruhe Institute of Technology (KIT)
      Fritz-Haber-Weg 6, 76131 Karlsruhe (Germany)
      E-mail: braese@kit.edu
      Homepage: http://www.ioc.kit.edu/braese

[b]   R. Israil, Dr. C. Riehn
      Department of Chemistry, Technische Universität Kaiserslautern (TUK)
      Erwin-Schrödinger-Str. 52, 67663 Kaiserslautern (Germany)

[c]   L. Schüssler, Prof. Dr. R. Diller
      Department of Physics, Technische Universität Kaiserslautern (TUK)
      Erwin-Schrödinger-Str. 46, 67663 Kaiserslautern (Germany)

[d]   E. K. Schneider, Dr. P. Weis, Prof. Dr. M. M. Kappes
      Institute of Physical Chemistry, Karlsruhe Institute of Technology (KIT)
      Fritz-Haber Weg 2, 76131 Karlsruhe (Germany)

[e]   Dr. M. Nieger
      Department of Chemistry
      University of Helsinki
      P. O. Box 55, Helsinki, 00014 (Finland)

[f]   Prof. Dr. M. M. Kappes
      Institute of Nanotechnology, Karlsruhe Institute of Technology
      Herman-von Helmholtz-Platz 1, 76344 Eggenstein-Leopoldshafen (Germany)

[g]   Dr. C. Riehn
      Research Center OPTIMAS
      Erwin-Schrödinger-Str. 46, 67663 Kaiserslautern (Germany)

[h]   Prof. Dr. S. Bräse
      Institute of Biological and Chemical Systems
      Functional Molecular Systems (IBCS-FMS) Karlsruhe Institute of Technology (KIT)
      Hermann-von-Helmholtz-Platz 1, 76344 Eggenstein-Leopoldshafen (Germany)

Chemistry–A European Journal

Full Paper
doi.org/10.1002/chem.202102341

Chemistry
Europe
European Chemical
Societies Publishing

conjugated tether. Both types of tethers have been reported for bimetallic ruthenium complexes,[7] whereas a conjugated tether allows an electronic communication between the metal centers and thus an alteration of the electronic properties of one or both metal centers.

Our research group has a long-standing interest in the chemistry of [2.2]paracyclophane (PCP) scaffolds for a diverse range of applications, including developing versatile PCP-derived planar chiral ligands and catalysts – employed most notably for various enantioselective transformations.[8] PCP is a co-facially stacked prochiral scaffold that displays unusual characteristics caused by transannular π-π electronic interactions of the benzene rings fixed in close proximity and exhibits unique stereochemical features on selective functionalization.[9] When employing carefully chosen transformations, different substituents can be positioned selectively either at only one or both benzene rings, i.e., mono-, and differently functionalized disubstituted PCP regioisomers including pseudo-*para*, -*ortho*, -*meta*, and -*geminal*, derivatives can be synthesized (Figure 1). The prefix pseudo refers to substituents positioned on different decks of the PCP scaffold. From a geometric point of view, the two moieties on PCP can be held parallel to each other, i.e., pseudo-*geminal*, anti-parallel in pseudo-*para* and variants of V-shaped geometries are obtained in pseudo-*ortho* and pseudo-*meta* position. The substitution pattern on PCP heavily influences the nature of the respective compound and even minor changes can alter its properties significantly.[10]

The application of PCP derivatives as chiral ligands or catalysts for stereoselective syntheses have been extensively investigated.[8b,11] Installation of (hetero)bimetallic centers using PCP as a bridging ligand can bring the metals in a well-defined and spatially-oriented relation to one another where M–M distance modulation and the extent of through-space electronic communication can be studied with regard to a structure-activity relationship and cooperative effects. Recent examples
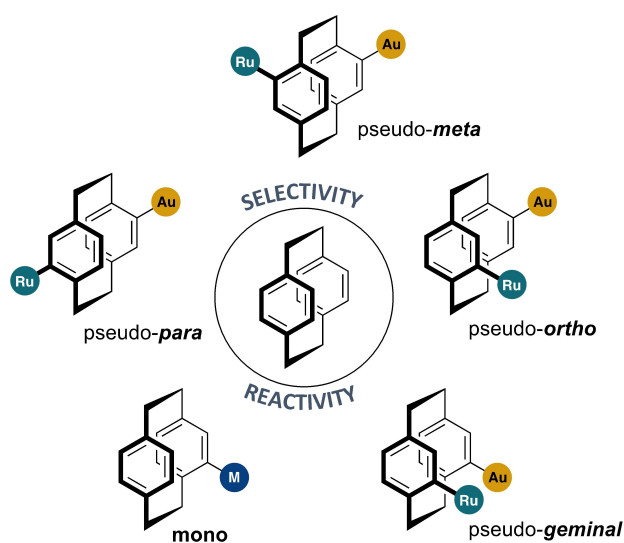
of PCP as a bridging ligand include distance-modulated cyclo-ruthenated complexes holding two ruthenium metal centers selectively either at only one or both decks with varying M–M distances.[12] PCP porphyrin conjugates allow convenient access to modular fixed-distance bimetallic Cu/Zn complexes.[13] In the context of π-electronic communication, "through-space" (i.e., π-stacking) via the co-facially stacked benzenes, various constitutional isomers of bis(ferrocenylvinyl)-substituted PCPs and diruthenium cyclophanyl complexes have been investigated and compared to their non-PCP analogues, where electron delocalization is a prominent contributing factor.[14] The regioselective substitution pattern of PCP can be used for M–M distance modulation. PCP-derived homobimetallic gold(I) complexes with varying intramolecular Au–Au distances based on the diphosphine ligands Ph$_2$-GemPhos and PhanePhos have previously been reported. By single crystal X-ray diffraction, the Au–Au distance in pseudo-*geminal* (2.98 Å) and pseudo-*ortho* (5.23 Å) position, as well as the respective P–P distances of 4.068 Å and 5.014 Å, in case of the corresponding ligands were found.[15] In this work, we report the modular synthesis of a series of cyclophanyl-derived mono- and M–M distance modulated (hetero)bimetallic complexes by combining Au(I) with Ru(bpy)$_2$ppy as a photosensitizer to explore the structure-activity relation and their synthetic applicability. Merging transition metal and photocatalysis to enable chemical synthesis with naturally abundant, visible light will significantly impact the emerging field of photocatalysis.[16]
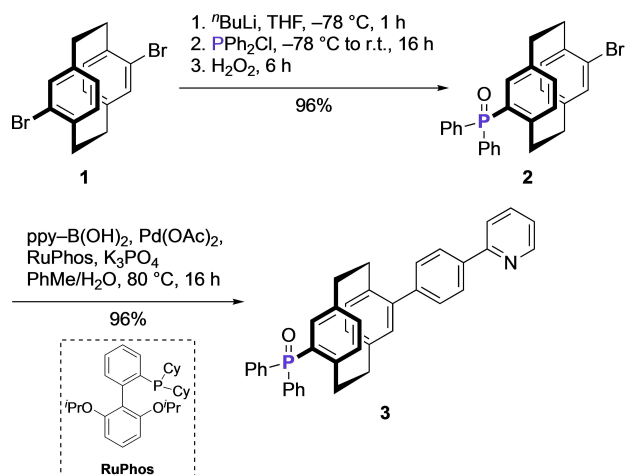
Results and Discussion

Synthesis: The Au(I) was to be incorporated by coordination with a triarylphosphine ligand while a cyclometallated phenyl-pyridine substituent would allow installation of the Ru(II).
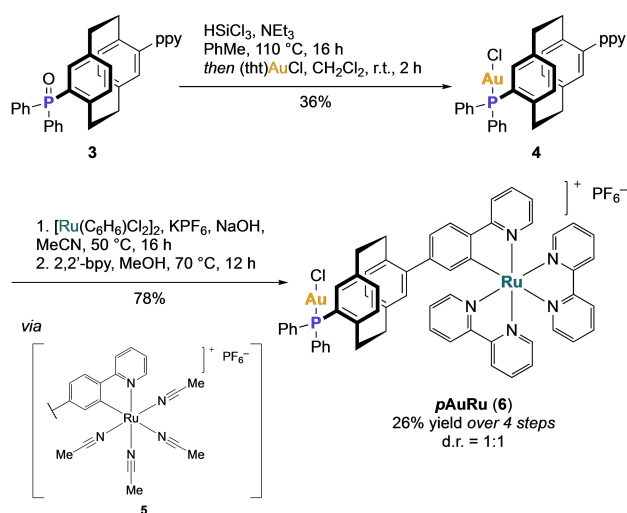
Starting from 4,16-dibromo[2.2]paracyclophane (**1**),[17] selective mono-lithiation and reaction with chlorodiphenylphosphine gave 4-bromo-16-diphenylphosphoryl[2.2]paracyclophane (**2**, Scheme 1). The phosphine is prone to oxidation in air and is rapidly converted to the phosphine oxide, making its isolation by column chromatography impractical. Therefore, before purification, the phosphine was oxidized with hydrogen peroxide to the corresponding phosphine oxide **2**, which simplified its isolation. Under optimized Suzuki-Miyaura reaction conditions, a new C–C bond to 2-phenylpyridine was formed. After two steps, compound **3** was obtained in 92% yield and bears both the phosphine oxide as a precursor for the selective binding of Au(I) and 2-phenylpyridine for the incorporation of Ru(II).[18]

Reduction of phosphine oxide **3** with trichlorosilane/triethylamine[11a] and reaction of the phosphine, which was obtained after rapid aqueous workup, with [(tht)AuCl],[19] gave compound **4** in 36% yield (Scheme 2).

Initial attempts to incorporate the Ru(II)(bpy)$_2$-structure into compound **4** were made by using [Ru(bpy)$_2$Cl$_2$] and silver(I) tetrafluoroborate as dechlorination agent to aid the cyclo-metallation reaction.[20] This method was unsuccessful, presumably due to the chlorine-abstracting properties of the silver salt,

Figure 1. Substitution pattern of [2.2]paracyclophane based monometallic complexes and bimetallic Au(I)/Ru(II) complexes.

Chemistry–A European Journal

Full Paper
doi.org/10.1002/chem.202102341

Chemistry Europe
European Chemical
Societies Publishing

Scheme 1. Selective mono lithiation followed by Suzuki-Miyaura reaction to obtain the intermediate ligand structure **3**. ppy = 2-phenylpyridine.

Figure 2. Crystal structures of **pAuRu** precursor 3. Displacement parameters are drawn at a 50% probability level.

Scheme 2. Incorporation of the gold(I) chloride and ruthenium(II) moiety to obtain **pAuRu** (**6**) as a 1:1 mixture of diastereomers. tht = tetrahydrothiophene, 2,2'-bpy = 2,2'-bipyridine.

the formation of a diradical, rotation, and subsequent ring closure), gave the pseudo-*meta* derivative **9** in 85% yield (Scheme 3, A).[17b,c,22] Similarly, pseudo-*ortho* derivative **10** was obtained by isomerization of **1** at 215 °C, in 85% yield. Followed by monolithiation and reaction with diphenylphosphine chloride gave 4-bromo[2.2]paracyclophane-12-diphenylphosphine oxide (**11**) in 61% yield (Scheme 3, B).[23]

The general synthesis route established for the preparation of **pAuRu** was also applied in the synthesis of the pseudo-*meta*, -*ortho*, and -*geminal* regioisomers, with slight variations. The Suzuki-Miyaura reaction conditions for both pseudo-*ortho* and -*geminal* derivatives **11** and **8** were modified since the standard protocol employing RuPhos as ligand only led to the isolation

which led to the decomposition of the gold moiety. The alternative approach that forgoes any dechlorination agent involves the formation of a cyclometallated tetraacetonitrile Ru(II) complex.[21] Complex **5** is formed by the reaction of ligand **4** with benzeneruthenium(II) chloride dimer in acetonitrile and sodium hydroxide as a base. Displacement of the labile acetonitrile ligands with 2,2'-bipyridine gave the final **pAuRu** complex **6** in 26% yield over four steps. The final complex **6** was obtained as a mixture of diastereomers with a planar chiral and a chiral-at-metal stereocenter. The molecular structure of the **pAuRu** precursors **3** was confirmed by single-crystal X-ray diffraction (Figure 2).

The selective bromination of 4-diphenylphosphonyl [2.2] paracyclophane (**7**), in pseudo-*geminal* position, gave compound **8** in 94% yield.[15c] Thermal isomerization of **8**, which involves the homolytic cleavage of one ethylene bridge (under
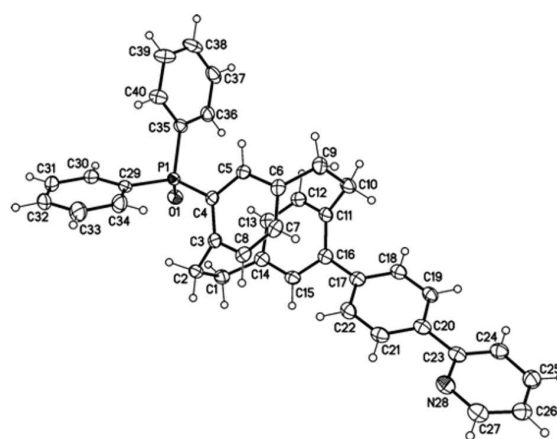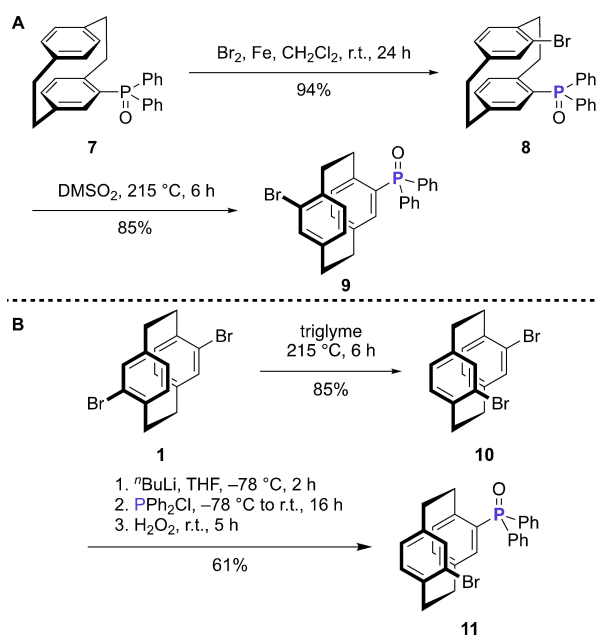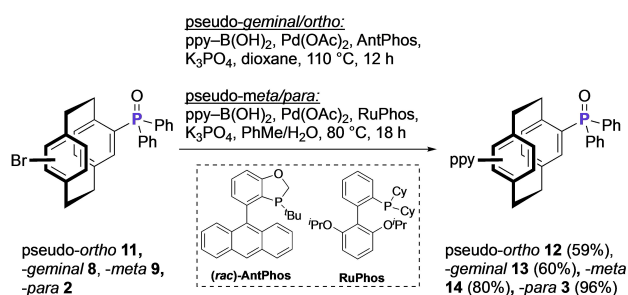

Scheme 3. Synthesis of compounds **8** and **9** towards **gemAuRu** and **mAuRu** (A). Synthesis of compound **11** via thermal isomerization of **1** towards **oAuRu** (B).

Chemistry–A European Journal

Full Paper
doi.org/10.1002/chem.202102341

**Chemistry
Europe**
European Chemical
Societies Publishing

of starting material. The use of (*rac*)-AntPhos, which is more adapted for the cross-coupling of sterically demanding substrates, gave the corresponding products **12** and **13** in 59% and 60% yield, respectively (Scheme 4).

Successive incorporation of the gold(I) chloride and ruthenium(II) bipyridyl moiety into the pseudo-*geminal* **13**, pseudo-*ortho* **12**, and pseudo-*meta* isomers **14** enabled to prepare a complete set of differently functionalized Au(I)/Ru(II) hetero-bimetallic complexes, ***gem*AuRu** (**18**), ***o*AuRu** (**19**), and ***m*AuRu** (**20**), with overall yields ranging from 10% to 28% (Figure 3). All **AuRu** isomers were obtained as diastereomeric mixtures with a d.r. = 1:1. For the detailed synthesis of the mono-metallic precursors **15**, **16**, and **17**, as well as ***gem*AuRu** (**18**), ***o*AuRu** (**19**), and ***m*AuRu** (**20**), see the Supporting Information. The respective mono-metallic **PCP-Au** (**21**) and **PCP-Ru** (**22**) were also prepared for their comparison with literature known complexes (Figure 4).

The molecular structure of the ***m*AuRu** precursor **14**, the ***o*AuRu** precursor **11** and monometallic **PCP-Au** (**21**) were confirmed by single-crystal X-ray diffraction (Figure 5). Single crystals of the final heterobimetallic **AuRu** complexes suitable for X-ray diffraction were not obtained.

Mass Spectrometric Analysis: The metal complexes **AuRu** (**6**, **18–20**), **PCP-Ru** (**22**) and **Ru(bpy)$_2$(ppy)** were analyzed by ESI-MS in their monocationic form, without counterions. In a second step, those were isolated in the ion trap and exposed to collision induced dissociation (CID) and photodissociation (PD). A qualitative examination of the **AuRu** complexes is exemplarily performed for the pseudo-*para* isomer ***p*AuRu** (**6**). All complexes were dissolved in acetonitrile and then injected by electrospray ionization into the mass spectrometer.

The molecular peaks for **[*p*AuRu]$^+$**, **[PCP-Ru]$^+$** and **[Ru-(bpy)$_2$ppy]$^+$** are found at m/z 1190, 774 and 568, respectively, and identified by their isotope patterns. CID of **[*p*AuRu]$^+$** (Supporting Information-Figure S89) takes place by two fragmentation pathways. The first pathway starts with the neutral loss of one bpy ligands forming the fragment with the highest intensity at m/z 1034. Subsequently [AuCl(PPh$_2$)-PCP-(ppy)Ru(bpy)]$^+$, either splits off a second bpy ligand giving m/z 878 or is subject to the loss of an HCl molecule at the ClAu(PPh$_2$)-PCP reactive site of the complex forming m/z 998. Since the latter peak appears only at a lower intensity, the loss of the second bpy seems to be favored. However, the loss of HCl takes place even after the loss of the second bpy ligand resulting in a peak at m/z 842. In each case, the proton (or H-atom) for the HCl loss probably stems from the spatially close phenyl group of the PPh$_2$ ligand or from the PCP ligand. Such cleavages are often observed in MS fragmentation.[24] Eventually, the loss of

Scheme 4. Suzuki cross-coupling conditions for incorporating the 2-phenyl-pyridine (ppy) moiety into pseudo-*geminal*/*ortho*- and pseudo-*meta*-/*para*-isomers.
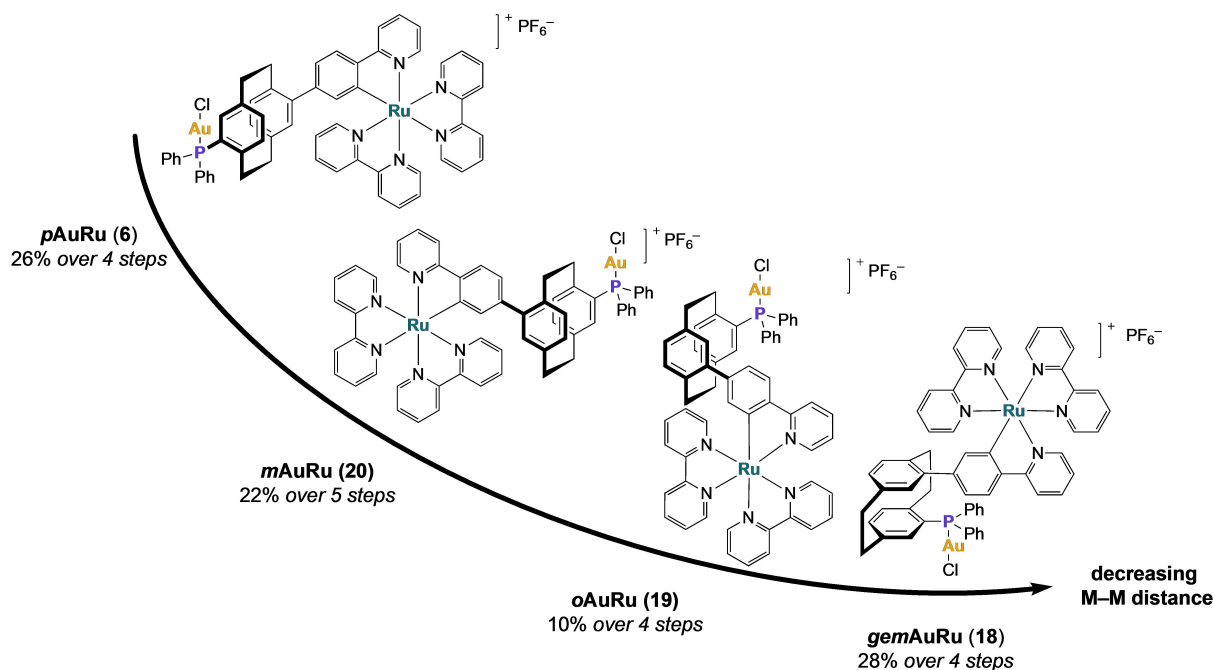
Figure 3. [2.2]Paracyclophane-based Au(I)/Ru(II) isomer set ***p*AuRu** (**6**), ***m*AuRu** (**20**), ***o*AuRu** (**19**), and ***gem*AuRu** (**18**) in order of decreasing M–M distance, based on the results obtained from IMS measurements (see Table 1).

Chemistry–A European Journal

Full Paper
doi.org/10.1002/chem.202102341

**Chemistry
Europe**
European Chemical
Societies Publishing

Figure 4. Monometallic complexes **PCP-Au** (**21**) and **PCP-Ru** (**22**).

Table 1. M-to-M distances of the global minima and the Boltzmann average of the possible rotamers.

entry	compound	Calculated CCS [Å^2][a,b]	Au–Ru distance [au][a]	Boltzmann Average [au][c]
1	*p*AuRu (6)	325	22.36	22.2
2	*m*AuRu (20)	311	15.49	18.5
3	*o*AuRu (19)	298	11.98	14.4
4	*gem*AuRu (18)	305	11.70	12.3

[a] Global minimal structure; [b] all calculated CCS are scaled by 0.89; [c] Boltzmann average of local minimum structures, 1.5 eV internal energy was assumed. 1 au = 0.529 Å.
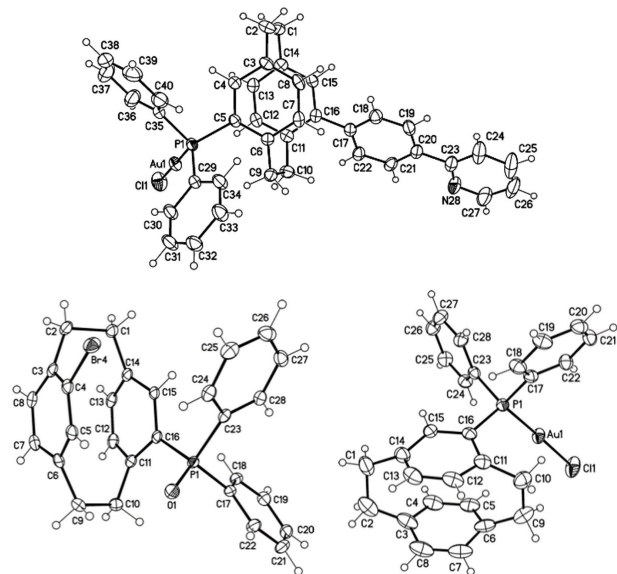

Figure 5. Crystal structures of *m*AuRu precursor **17** (top), *o*AuRu precursor **11** (bottom left) and **PCP-Au** (**21**, bottom right). Displacement parameters are drawn at a 50% probability level in case of **17** and **11**, and at a 30% probability level in case of **21**.

the Au atom and a Ph substituent leads to the species [[(PPh)-PCP-ppy)Ru]-H]$^+$ appearing with low intensity at m/z 568.

The second pathway, marked by the peak at m/z 670, is assigned to [C$_8$H$_7$-(ppy)Ru(bpy)$_2$]$^+$, which is formed by the cleavage of the aliphatic group of PCP. The further loss of the bpy ligand leads to [C$_8$H$_7$-(ppy)Ru(bpy)]$^+$ at m/z 514 and in combination with the decomposition of the PCP residual (C$_8$H$_7$) to the fragment at m/z 412. All fragment assignments are summarized in Supporting Information-Table 1.

The photofragmentation of [*p*AuRu]$^+$ again leads to two fragmentation channels: either the cleavage of a bpy ligand or the -C$_8$H$_7$-(PPh$_2$)-AuCl unit. Judging by the intensity differences, the disintegration to [AuCl(PPh$_2$)-PCP-(ppy)Ru(bpy)]$^+$ (m/z 1034) is preferred over [C$_8$H$_7$-(ppy)Ru(bpy)$_2$]$^+$ (m/z 670). In comparison to CID, both species match the above discussed fragmentation pathways, whereby the peak at m/z 1034 only appears with very low intensity by CID. The isolation and fragmentation of [**PCP-Ru**]$^+$ (Supporting Information-Figure S91) leads to only one fragment at m/z 670, which is assigned to [C$_8$H$_7$-(ppy)

Ru(bpy)$_2$]$^+$ and formed as discussed before. To confirm the assignment, the ions related to m/z 670 were isolated in a MS^2 step and subjected to fragmentation. The resulting fragments at m/z 514 and 412 match the previously discussed fragmentation pathway. However, the photoinduced dissociation only leads to the fragment at m/z 670. The CID fragmentation of [**Ru(bpy)$_2$ppy**]$^+$ (Supporting Information-Figure S93), results in the loss of one bpy ligand leading to the species [Ru(bpy)ppy]$^+$ at m/z 412 and the subsequent attachment of one H$_2$O molecule forms [Ru(bpy)ppy(H$_2$O)]$^+$ at m/z 430, which is a common ion-molecule reaction for undercoordinated Ru^{II} complexes in ion traps. The photodissociation approach shows barely any fragmentation yield, probably since the necessary dissociation energy for the bidentate ligands cannot be achieved by one-photon absorption processes.

Ion Mobility Spectrometry: A combination of quantum chemical calculations and ion mobility spectrometry (IMS) was used to obtain structural parameters and estimate the M–M distances of the AuRu complexes (Table 1).

Trapped ion mobility spectrometry coupled with a time of flight mass spectrometer (timsTOF) was performed to determine the collision-cross sections (CCS) of the **AuRu** ions in the gas-phase (Figure 6).

The obtained CCS follow the order *p*AuRu > *m*AuRu > *o*AuRu ≈ *gem*AuRu and are qualitatively consistent with calculated CCS of the complexes (Figure 7, obtained by trajectory calculations with the IMoS package).[25]

Additionally, IMS allows the differentiation of isomers and conformers that differ by less than 0.5% in CCS. The diastereomeric nature of the **AuRu** complexes indicated by a double signal set in NMR spectroscopy was also confirmed by the two peaks present in each mobilogram.

Ground State Studies: Electronically excited states, which are essential in photoredox chemistry, are generated by the light absorption of a molecule in the ground state. Selective and efficient irradiation and the evaluation of redox properties are essential for understanding and ultimately, applying new photoredox catalysts. For this purpose, absorption and emission spectroscopy and cyclic voltammetry were performed.
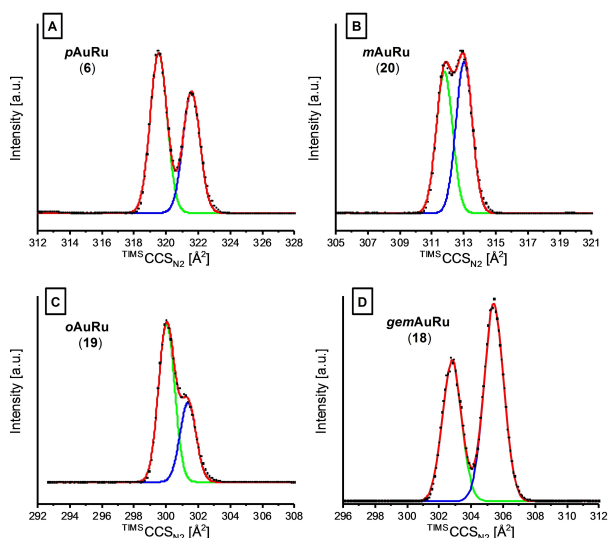
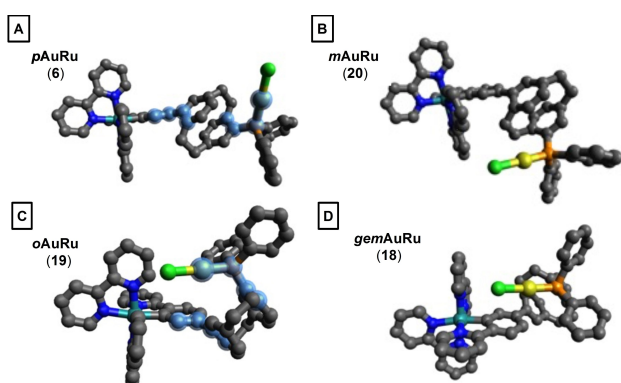**Figure 6.** Mobilograms of the **AuRu** isomers obtained from IMS.

Figure 7. Global minimal structures obtained from DFT-geometry optimizations by varying all degrees of freedom (see Supporting Information).
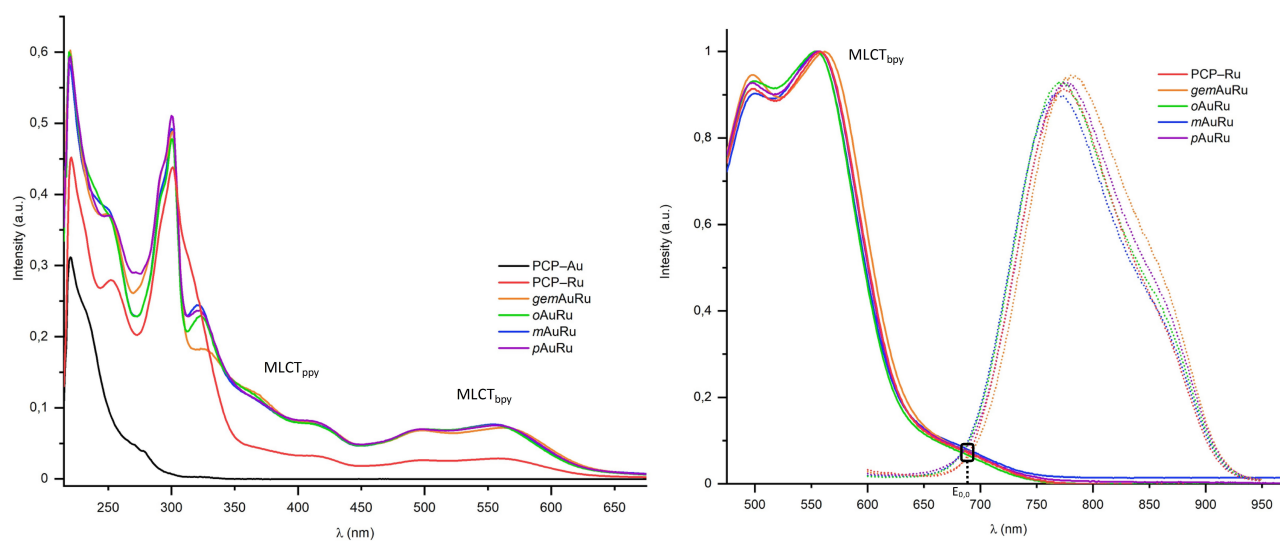
Absorption/Emission Spectroscopy

The room temperature absorption spectra of monometallic and heterobimetallic Au(I)/Ru(II) PCP complexes are shown in Figure 8. The UV region below 310 nm is dominated by spin allowed ligand centered (LC) transitions and additional interligand (ppy – bpy) transitions. Additionally, the monometallic **PCP-Ru** (**22**) and the heterobimetallic **AuRu** isomers **6** and **18–20** show an additional band at 320 nm, where the PCP backbone is likely to contribute.[26] Examining the lower energy absorption bands reveals a large spectral envelope that arises from the cyclometalated 2-phenylpyridine ligand. The two absorption bands in the region between 350–450 nm and 450–600 nm result from metal-to-ligand charge transfer (MLCT) transitions.[20b] The MLCT bands show similarly high molar extinction coefficients for all heterobimetallic **AuRu** isomers while being substantially more prominent than the monometallic **PCP-Ru** (Table 2). The first band can be assigned to an MLCT from the ruthenium center to the cyclometalating 2-phenylpyridyl ligand, whereas the band at higher wavelengths is primarily localized on the bipyridyl ligands, indicating a delocalization of the LUMO mostly on the bipyridyl ligand, whereas the HOMO is most likely localized on the cyclometalating phenylpyridyl.[20b,27]

The emission spectra were recorded under argon atmosphere at 20 °C under excitation at wavelengths defined by the absorption maximum at 495 nm (Figure 8, right). This produces an emission band with a substantial Stokes shift at 795 nm. The excited-state energy of the first singlet excited state $E_{0,0}$ was estimated from the crossing point between absorption and emission profile.[28] This energy refers to the transition between the lowest energy vibrational state ($\nu = 0$) of S_1 to $\nu = 0$ of S_0. Alternative methods to approximate this value use the earliest onset (highest energy) of fluorescence, the midpoint between emission and absorption maxima (one-half Stoke-shift), or the

Figure 8. Normalized absorption (solid lines) and emission (dotted lines) spectra of **PCP-Au** (**21**), **PCP-Ru** (**22**), and **AuRu** isomers **6** and **18–20**. ($\lambda_{ex} = 495$ nm, 100 µм in CH$_2$Cl$_2$, 20 °C).

Chemistry–A European Journal

Full Paper
doi.org/10.1002/chem.202102341

Chemistry Europe
European Chemical
Societies Publishing

fluorescence maximum. Each method is an approximation and is likely to over- or underestimate the value for $E_{0,0}$. In combination with the ground state reduction and oxidation potentials, which are obtained from cyclic voltammetry (see below), it is used to estimate the excited state potentials E*.

Action Spectroscopy in Gas-phase and TD-DFT Calculations

Ion trap UV photodissociation (UV-PD) spectroscopy in gas phase is an established technique, even though its application was realized with different experimental setups and primarily used for the investigation of biomolecular systems.[29] It has recently been applied to study metal complexes or aggregates.[24,30] However, studies for multimetallic, especially heterometallic, molecular systems are still scarce in this field.[24,31] In order to determine the intrinsic UV spectra devoid of counterions and solvent effects, UV photodissociation (UV-PD) spectra of the pseudo-*para* complex **6**, the monometallic complex **22** and [Ru(bpy)$_2$ppy]$^+$ were recorded. After electrospray ionization and mass-selective ion-trap isolation at room temperature the corresponding cations [*p*AuRu]$^+$, [PCP-Ru]$^+$ (**22**) and [Ru(bpy)$_2$ppy]$^+$ were examined at m/z 1190, 774 and 568.

UV-PD spectra represent gas phase *action spectra* recorded by UV laser irradiation of the mass-selected and stored species in an ion trap by monitoring their relative photofragment yield (since photoexcitation usually leads to dissociation if the photon energy exceeds possible fragmentation barriers) as a function of laser wavelength. Here, [*p*AuRu]$^+$ shows two bands in the CT region (>400 nm) and more intense bands at 350 nm, 295 nm, and 260 nm. The UV-PD spectrum of [PCP-Ru]$^+$ exhibits similar band positions as [*p*AuRu]$^+$ below 400 nm, however, the bands at 350 nm and 260 nm appear with lower intensity (Supporting Information-Figure S97). The UV-PD spectrum of [Ru(bpy)$_2$ppy]$^+$ only shows a band at 295 nm with low intensity. For [PCP-Ru]$^+$ and [Ru(bpy)$_2$ppy]$^+$ above 400 nm the fragment yield was too low for analysis, possibly due to the relatively high activation barriers for dissociation, so that the UV-PD spectra could not be obtained in those CT regions.

A comparison of the gas phase to the solution phase spectra reveals similarity for all studied species with the strongest band close to 300 nm. Remarkably, for [*p*AuRu]$^+$ a second peak (red-shifted to 350 nm) appears in the gas phase spectrum resembling the double-peak structure observed in other Ru^{II} complexes in the gas phase.[32] It could originate from the shoulder or a small peak observed at 320 nm in solution. However, this feature does not appear in the spectrum of the [Ru(bpy)$_2$ppy]$^+$ species and is related to the PCP and/or the PPh$_2$AuCl unit and constitutes an interesting target wavelength for ultrafast pump-probe studies (see below).

Quantum-chemical calculations based on time-dependent density functional theory (TD-DFT) using the hybrid functional (CAM-)B3LYP with the cc-PVT(D)Z basis set (ECP for Ru and Au, Stuttgart97) were employed to get insight into the underlying electronic transitions. The B3LYP functional delivers satisfying results for Ru(II) polypyridyl complexes,[33] while CAM-B3LYP corrects for the long/short range correlation issue of larger molecules.[34] From these calculations, theoretical absorption spectra were obtained for all conformational isomers of both diastereomers of [*p*AuRu]$^+$ (**6**) and plotted in Figure 9 and Supporting Information-Figure S101. The spectra are remarkably similar to each other and display only a slight variability in the shoulder at 320 nm. Moreover, the spectra mimic the experimental solution spectra in the short wavelength region quite nicely, although the CT region, especially above 500 nm is not well reproduced. However, the calculated spectrum using the B3LYP functional shows more similarity to the UV-PD gas phase spectrum and reproduces its strong band at 350 nm (Supporting Information-Figure S99).

The type of transition is identified by visualizing the involved molecular orbitals (MOs, Supporting Information-Figure S104). The absorption and UV-PD spectrum of [*p*AuRu]$^+$ and the calculated transitions in form of vertical sticks are shown in Figure 10. The broad bands in the experimental data, their intensity, and shape depend critically on the calculated "density", position and oscillator strength of these electronic transitions. The percentages of the coupled ground and excited state MOs for each transition is shown in Supporting Information-Table S7. Based on the contribution of the involved MOs the type of transition can be estimated. For [*p*AuRu]$^+$ only transitions possessing an oscillator strength of ≥ 0.03 and MOs with a weight ≥ 10% were considered. The bands in the CT region (370 nm–560 nm) are assigned to the states S5, S6, S22, and S29 and characterized as MLCT transition, where the electron density from Ru is moved partially to the ligands bpy and bpy' (Supporting Information-Figure S103, structural breakdown).

The transitions for the band around 360 nm cannot be clearly and uniformly assigned due to the low contribution of the involved MOs. However, S38, S39 and S40 suggest a MLCT transition partially from **AuRu** onto the ligands coordinated at Ru (ppy, bpy, bpy'). The transition S45 at 345 nm shows ILCT (interligand charge transfer) character, where the electron
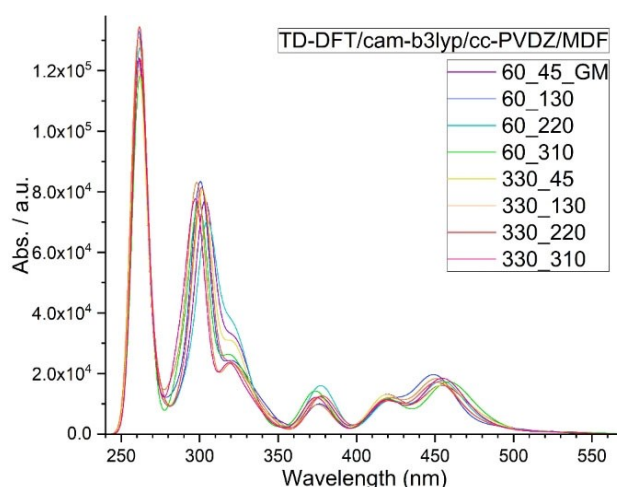

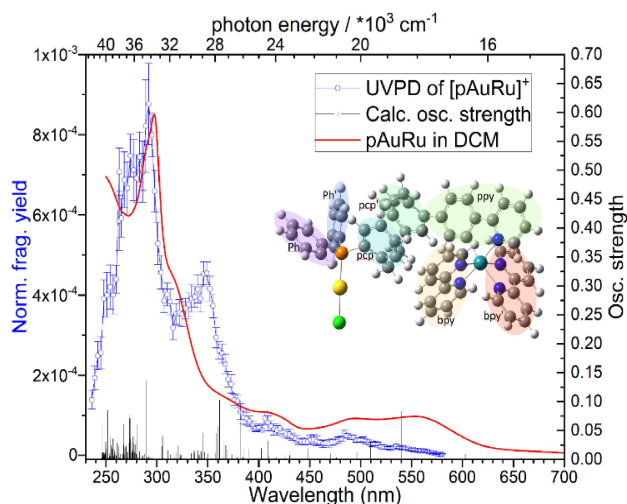**Figure 9.** Calculated absorption spectra of the eight conformers of one diastereomer of [*p*AuRu]$^+$.

Figure 10. Gas phase UV-PD spectrum (blue) and calculated transitions (stick) of [*p*AuRu]$^+$ calculated with B3LYP, as well as the liquid phase absorption spectrum in CH$_2$Cl$_2$ (red) of *p*AuRu (**6**). The different ligands of the complex are marked with their abbreviations.

density moves from a ligand coordinated at Au to the ppy ligand. In the UV-PD gas phase spectrum of *p*AuRu (**6**), a weak shoulder appears around 310 nm. This is assigned to the transitions S79 and S80, characterized as MLCT involving Au and the ligands ppy, bpy and bpy'. This wavelength region was also used for transient absorption spectroscopy in this work (see below). The calculation for S98 did not result in a clear type of this transition. However, an LC transition is assigned to S111. The remaining states do not possess MOs with a significant contribution, so that the characterization of those transitions is unclear. However, the states under 300 nm strongly suggest ILCT and LC transitions. The calculations with the CAM-B3LYP functional (Figure 9, Supporting Information-Figure S107–111,

Supporting Information-Table S10–S12) deliver a better description of the MOs and the according transitions. By and large, their assignment follows those obtained with the B3LYP functional. However, the calculated spectrum using CAM-B3LYP is blue shifted in comparison to the results presented in Figure 10. The MLCT transitions involving Au appear at 254 nm, the ILCT transitions involving PCP at 280 nm and the MLCT transitions involving Ru at >300 nm. In summary, the theoretical analysis by TD-DFT agrees only partially with the experimental results but allows for adequate and generic assignment of the transitions in order to characterize the observed bands in Figures 8, and .

Cyclic Voltammetry

The redox behavior of **PCP-Ru** (**22**) and all **AuRu** isomers **6** and **18**–**20** consists of a reversible metal-based oxidation process in the range of +0.26−+0.51 V, which is assigned to the Ru$^{II/III}$ redox couple (Figure 11, left). An irreversible ligand-based reduction process at −1.67−−2.24 V is observed and can be ascribed to reducing the bipyridyl ligands. The anionic and electron-rich character of the 2-phenylpyridyl ligands makes its reduction more complicated such that it occurs at lower reduction potentials.

CV measurements of **PCP-Ru** (**22**) and *m*AuRu (**20**) were conducted at different scan rates (see Supporting Information-Figure S77 and S78). The peak current was plotted against the square root of the scan rate to obtain the Randles-Sevcik plots (see Supporting Information-Figure S79 and S80).[35] The linear relationship between peak current and the square root of the scan rate indicates that the oxidation process is diffusion controlled. The measurements were only conducted for the monometallic **PCP-Ru** (**22**) and heterobimetallic complex *m*AuRu (**20**). Similar behavior is assumed for all other **AuRu** isomers.
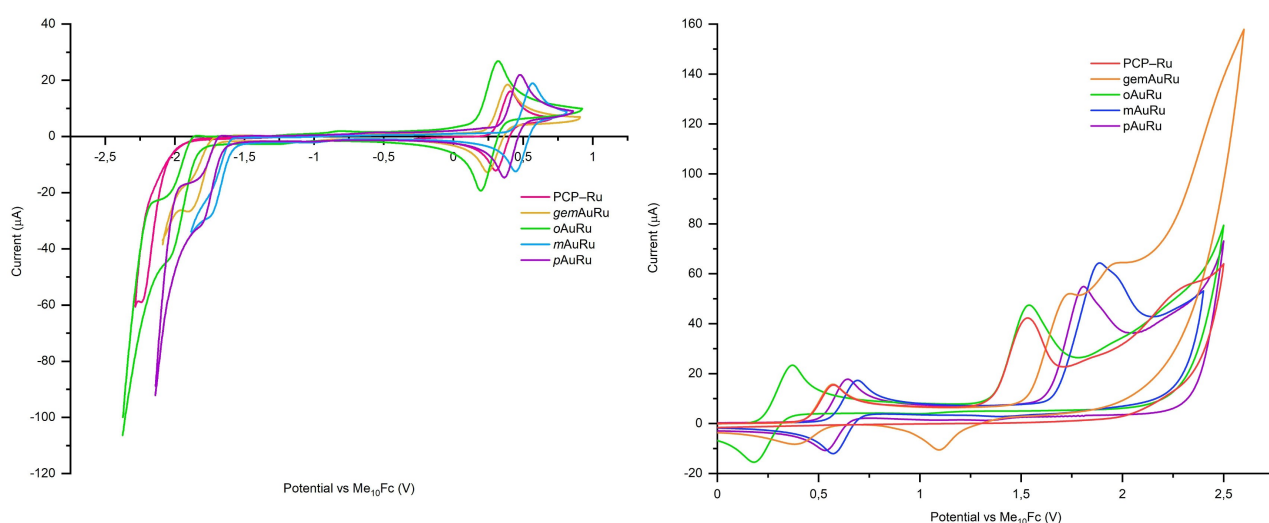

Figure 11. Cyclic voltammograms of **PCP-Ru** (**22**) and **AuRu** isomers **6** and **18**–**20** (left) and CV spectra of the second oxidation process (right) (0.1 M ^{n}Bu$_4$NPF$_6$, CH$_2$Cl$_2$, 100 mV/s).

Chemistry–A European Journal

Full Paper
doi.org/10.1002/chem.202102341

Chemistry Europe
European Chemical
Societies Publishing

A second and third oxidation process takes place in the range of 1.45–1.90 V (Figure 11, right) and are irreversible. Upon repeated cycles, an insulating layer forms on the electrode surface, which causes a decrease in current intensity from cycle to cycle. These oxidation processes can either be attributed to a $Ru^{III/IV}$ oxidation or ligand decomposition, displayed by cyclometallated complexes.[36] Additionally, the (electro)chemical oxidation of [2.2]paracyclophane and some of its derivatives is well established and leads to the formation of benzyl radical/benzyl cation intermediates under C–C bond scission of the ethano bridges. The highly reactive intermediate readily reacts either with itself or other molecules to form an insulating polymeric species.[9d,37] The combined data obtained from absorption/emission spectroscopy and cyclic voltammetry measurements are summarized in Table 2. Most ground state parameters such as absorption maxima (λ_{max}^{abs}), molar extinction coefficient (ε_{495nm}), HOMO-LUMO gap ($\Delta E_{HOMO-LUMO}$), and $E_{0,0}$ show only slight deviations among the **AuRu** isomers **6** and **18**–**20**. The oxidation and reduction potentials $E_{1/2}^{ox}$ and $E_{1/2}^{red}$ indicated a significant M–M interaction.

The first oxidation potential describes the oxidation of Ru^{II} to Ru^{III}, whereas the reduction takes place on the 2-phenyl-pyridine moiety of the **AuRu** isomers. The order for oxidation and reduction potential is mirrored, where the most substantial oxidation potential and therefore the weakest reduction potential are found for **mAuRu** (**20**, **Equation (1)**).

$$E_{ox}^{\,mAuRu} > E_{ox}^{\,pAuRu} > E_{ox}^{\,gemAuRu} > E_{ox}^{\,oAuRu}$$

$$E_{red}^{\,oAuRu} < E_{red}^{\,gemAuRu} < E_{red}^{\,pAuRu} < E_{red}^{\,mAuRu}$$

Equation 1 Order of oxidation (top) and reduction potentials (bottom) of **AuRu** isomers **6** and **18**–**20** from strongest to weakest (left to right).

These results can be rationalized by transannular and through-space interactions between the gold and ruthenium centers. In pseudo-*para* position, electron-donation of the gold moiety onto the ruthenium center is possible by trans-annular communication and leads to an increase of $E_{1/2}^{ox}$ by 0.09 V. This type of communication is most pronounced in pseudo-*ortho* position, which leads to an oxidation potential which is 0.10 V less than the monometallic **PCP-Ru** (**22**). It is least pronounced in the pseudo-*meta* position, which accounts for a difference of 0.15 V compared to **PCP-Ru** (**22**), such that the value of $E_{ox}^{\,oAuRu}$

is 0.25 V less than for **mAuRu** (**20**). The oxidation potential of **gemAuRu** (**18**) indicates a very weak interaction between the gold and ruthenium centers, which is a deviation of 0.04 V compared to the monometallic **PCP-Ru** (**22**).

From the obtained oxidation and reduction potentials combined with $E_{0,0}$, an approximate value for the excited state potentials E* can be obtained and summarized in Table 2.

The excited state reduction potential E_{ox}* shows that both monometallic catalyst **PCP-Ru** (**22**) and the **AuRu** isomers **6** and **18**–**20** are considerably stronger reducing agents in their excited than in their ground state. The order of redox potentials is consistent with the corresponding ground state values, where **oAuRu** (**19**) is the most potent reducing agent and **mAuRu** (**20**) the weakest. Photoinduced reduction with either **PCP-Ru** (**22**) or any of the **AuRu** isomers is unfavorable since E_{red}* is either negative or has small positive values. This is in agreement with the proposed mechanisms presented in the literature where it is shown that the excited state of Ru undergoes oxidative quenching by the aryldiazonium salt.[38]

Ultrafast Transient Absorption Spectroscopy: As a first step to further unravel the M–M interactions via femtosecond (fs) transient absorption spectroscopy, the photo-induced dynamics of **pAuRu** (**6**) was compared to the monometallic **PCP-Ru** (**22**) and **Ru(bpy)₂ppy**.[20b] For **pAuRu** (**6**) in CH_2Cl_2 no significant difference was observed for the photoinduced dynamics when excited at 405 nm or 495 nm (Figure 12A, Supporting Information-Figure S81A). Comparison to **Ru(bpy)₂ppy** in CH_2Cl_2, excited at 405 nm and 312 nm (Supporting Information-Figure S81B, C), also shows no change in dynamics. Thus, under excitation in the MLCT-bands around 405 nm and 495 nm no significant influence of the PCP-Au-moiety on the photoinduced dynamics of **pAuRu** (**6**), but only the dynamics of the Ru-moiety was observed. However, when **pAuRu** (**6**) is excited at 312 nm, an impact on the difference spectra is obvious (Figure 12A and B). Even more striking, the difference spectra of **PCP-Ru** (**22**) in CH_2Cl_2 excited at 312 nm (Figure 12C) clearly differ from those of **pAuRu** (**6**) as well as **Ru(bpy)₂ppy**. Thus, in contrast to excitation at 405 and 495 nm, excitation at 312 nm dramatically changes the kinetics in **pAuRu** (**6**) and **PCP-Ru** (**22**), although in a different manner. In other words, the addition of the Au-moiety (which does not exhibit an absorption band at 312 nm) to **PCP-Ru** (**22**) (which does exhibit an absorption band at 312 nm, Figure 8),[18b] leads to a significant and non-additive change of the excited state dynamics.

Table 2. Summary of ground-state and excited-state properties of **PCP-Ru** and **AuRu** isomers.

entry	compound	λ_{max}^{abs} [nm]	ε_{495nm} [10^5 M^{-1} cm^{-1}]	$E_{1/2}^{ox}$ [V]	$E_{1/2}^{red}$ [V]	$\Delta E_{HOMO-LUMO}$ [eV]	λ_{max}^{em} [nm]	$E_{0,0}$ [eV]	E_{ox}* [V]	E_{red}* [V]
1	**PCP-Ru** (**22**)	558	3.49	0.36; 1.45	−2.24	2.60	774	1.81	−1.45	−0.43
2	**gemAuRu** (**18**)	562	9.07	0.32; 1.53	−1.80	2.10	781	1.79	−1.47	−0.01
3	**oAuRu** (**19**)	554	9.30	0.26; 1.60	−1.95	2.20	774	1.82	−1.56	−0.13
4	**mAuRu** (**20**)	554	9.18	0.51; 1.79	−1.67	2.20	769	1.81	−1.30	0.14
5	**pAuRu** (**6**)	557	9.31	0.42; 1.86	−1.75	2.20	777	1.81	−1.39	0.06

λ_{max}^{abs} = absorption maximum of $ML_{bpy}CT$, ε_{495nm} = molar extinction coefficient, $E_{1/2}^{ox}/E_{1/2}^{red}$ = ground state oxidation/reduction potential, E_{ox}*/E_{red}* = excited state oxidation/reduction potential, $\Delta E_{HOMO-LUMO}$ = HOMO-LUMO gap energy, λ_{max}^{em} = emission maximum, $E_{0,0}$ = excited state energy of the first singlet excited state S_1 (zero-zero transition energy).
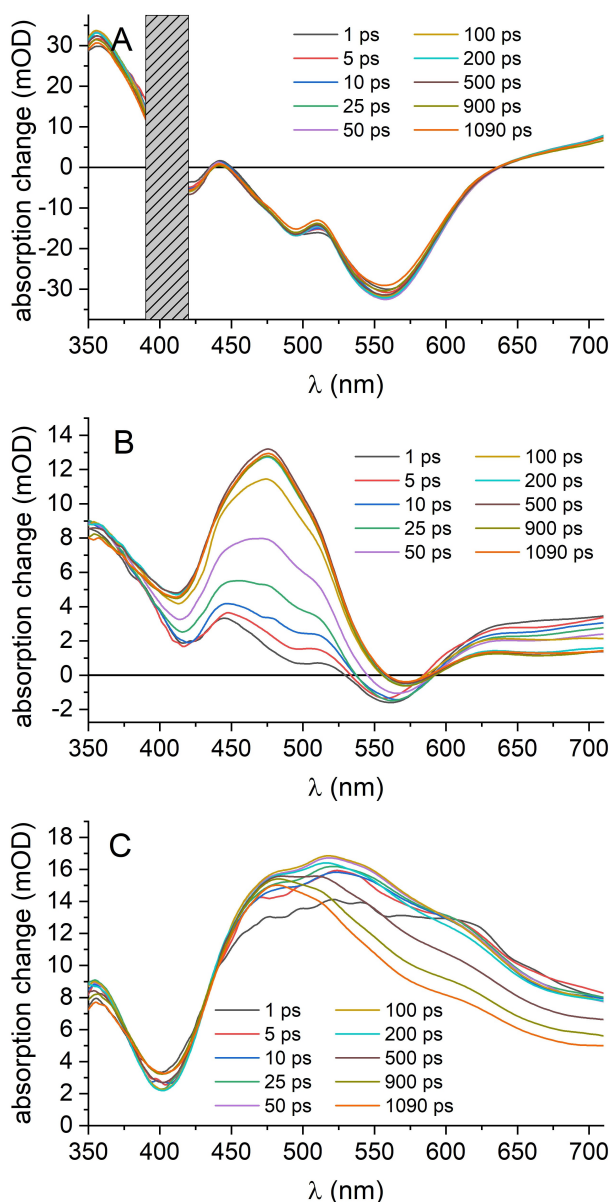
Chemistry–A European Journal

Full Paper
doi.org/10.1002/chem.202102341

Chemistry
Europe
European Chemical
Societies Publishing

Figure 12. Difference spectra at selected delay times for *p*AuRu (**6**) in CH$_2$Cl$_2$ excited at 405 nm (A), *p*AuRu (**6**) in CH$_2$Cl$_2$ excited at 312 nm (B) and **PCP-Ru** (**22**) in CH$_2$Cl$_2$ excited at 312 nm (C). The grey area in A from 390 nm to 420 nm is excluded from data analysis due to pump scattering.

Independent of excitation wavelength (312, 405, 495 nm), all measured complexes in Figure 12 and Supporting Information-Figure S81 show the excited state absorption (ESA) band at around 355 nm which is typical for the ^{3}MLCT excited states of Ru(II)-bipyridyl complexes.[33,39] After a strong instantaneous rise the signal shows only small amplitude changes.

*p*AuRu (**6**) excited at 405 nm and 495 nm as well as **Ru(bpy)$_2$ppy** excited at 405 nm and 312 nm (Figure 12A, Supporting Information-Figure S81A, B, C) show the typical instantaneous ground state bleach (GSB) of Ru(II)-bipyridyl complexes (around 400–625 nm), paralleled by superimposed (^{3}MLCT-) ESA bands on both sides of the spectrum.[27b,33] For wavelengths above about 600 nm, ESA contributions from

^{3}MLCT[33] and a ^{3}MC excited state[39] are expected. After instantaneous rise the signals in this region show only small amplitude changes over the entire time range of 1.1 ns.

For *p*AuRu (**6**) excited at 312 nm (Figure 12B) instead of the GSB a strong ESA band with maximum at 475 nm is observed. This ESA band is distinctively separated from the ^{3}MLCT-ESA band around 355 nm by a local minimum at 410 nm and exhibits a completely different temporal evolution for wavelengths above 390 nm: After a decent rise within ca. 1 ps the signal strongly increases to maximum with $t_3 = 68$ ps (according to global analysis, see Table 3 and Supporting Information) and remains basically constant up to 1 ns. Between 528 and 592 nm a small residual GSB signal is present with kinetics dominated by the overlapping ESA. The ESA band for wavelengths above 592 nm is probably caused by the ^{3}MLCT and ^{3}MC-excited states, in analogy to Ru(II)-polypyridine complexes.[33,39] This band partially decays as well with τ_3. Thus, τ_3 seems to represent the depopulation of the ^{3}MC-excited states and the simultaneous population of a state X (which is not yet specified in more detail) around 475 nm (see A$_3$ in Supporting Information-Figure S83D). Therefore, we propose an intersystem crossing (ISC) or internal conversion (IC) process from the ^{3}MC excited states to an unknown state X with τ_3. This process is not observed for *p*AuRu (**6**) excited at 405 nm and 495 nm or **Ru(bpy)$_2$ppy**, excited at 405 and 312 nm.

The monometallic **PCP-Ru** (**22**) excited at 312 nm (Figure 12C) only shows a broad ESA band besides the ^{3}MLCT-ESA-band at 355 nm and no bleach band in the examined spectral window. Inspection of Figure 12B and C (and decay associated spectra in Supporting Information-Figure S83D and E) reveal that the spectro-temporal evolution is significantly different from that in *p*AuRu (**6**), but bears also characteristic similarities: (i) In **PCP-Ru** (**22**) the same band (at 475 nm) as in *p*AuRu (**6**) is formed, but much faster, i.e. with a strong instantaneous component (ca. 70%, see Supporting Information-Figure S83E) and two weak components ($\tau_1 = 1.1$ and $\tau_3 = 42$ ps), and a lifetime much larger than 1 ns. However, signal decay in the region of ^{3}MC absorption in synchrony with the ultrafast rise of the band at 475 nm is not observed, possibly due to non-sufficient time resolution. (ii) In contrast to *p*AuRu (**6**) in **PCP-Ru** (**22**) an additional strong band at around 565 nm is formed concomitantly with the band at 475 nm but lifetime of about 2 ns.

The process of the proposed ISC or IC with τ_3 in *p*AuRu (**6**) is not distinctively observed in **PCP-Ru** (**22**), where the same state X seems to be populated much faster, and a strong ESA absorption around 565 nm indicates the formation of another

Table 3. Time constants resulting from a global analysis of femtosecond transient absorption data in CH$_2$Cl$_2$ (see Supporting Information).

entry	compound	λ_{ex} [nm]	τ_1 [ps]	τ_2 [ps]	τ_3 [ps]	τ_4 [ns]
1	**Ru(bpy)$_2$(ppy)**	405	0.7 ± 0.2	17 ± 3	/	/
2	*p*AuRu (**6**)	405	1.0 ± 0.3	14 ± 3	/	/
3	*p*AuRu (**6**)	495	1.2 ± 0.2	14 ± 1	/	/
4	*p*AuRu (**6**)	312	0.3 ± 0.1	5.5 ± 1.0	68 ± 3	/
5	**PCP-Ru (22)**	312	1.1 ± 0.2	8 ± 2	42 ± 6	(~ 2)

Chemistry–A European Journal

Full Paper
doi.org/10.1002/chem.202102341

Chemistry
Europe
European Chemical
Societies Publishing

state, possibly quenched in *p*AuRu (**6**). This highlights the influence of the Au-moiety when *p*AuRu (**6**) is excited at 312 nm. Analogous investigations are in progress to analyze the underlying processes in the isomers **6** and **18–20**, in particular with respect to the varying M–M-distance.

Ultrafast Transient Photodissociation Spectroscopy: In order to obtain intrinsic ultrafast dynamics we have applied our technique of *pump-probe photodissociation spectroscopy* (τ-PD) to the isolated ions [***p*AuRu**]$^+$ (**6**, m/z 1190) and [**PCP-Ru**]$^+$ (**22**, m/z 774) in an ion trap at room temperature, with the aim to discern the influence of the PPh$_2$AuCl moiety on the [**PCP-Ru**]$^+$ unit.[32] We have restricted ourselves to the investigation of the pseudo-*para* isomer, since its observed photocatalytic efficiency was the highest (Table 4) and hence dynamic effects of energy or excitation transfer from the Ru antenna unit to the reactive Au center are expected. Using τ-PD we record ultrafast dynamics of species produced by electrospray-ionization with subsequent mass-selection in an ion trap mass spectrometer after resonant photoexcitation in gas phase by monitoring their photofragment yield as a function of resonant *pump* (UV)-non-resonant-*probe* (NIR) time delay.

Here, the pump wavelength for excitation for both, [***p*AuRu**]$^+$ (**6**) and [**PCP-Ru**]$^+$ (**22**) was set to 350 nm, which stems from the assignment of this peak in the gas phase spectrum (Supporting Information-Figure S100) to a band containing "cyclophane and phenyl-pyridine (π→π*) transitions" (see above). Note, that we assume that in the solution spectra a similar transition is observed at 312 nm (as a shoulder) and subsequently explored by ultrafast transient absorption as described above. However, the transients obtained for the gas phase by τ-PD (Supporting Information-Figure S110–S114) give a relatively limited picture and exhibit for both species a fast sub-picosecond relaxation, possibly internal vibrational redistribution (IVR, with τ$_1$∼0.5 ps +/− 0.05 and 0.4 ps +/− 0.04, for [***p*AuRu**]$^+$ (**6**) and [**PCP-Ru**]$^+$ (**22**), respectively; Figure 13 and Supporting Information-Table S8) followed by stabilization of a
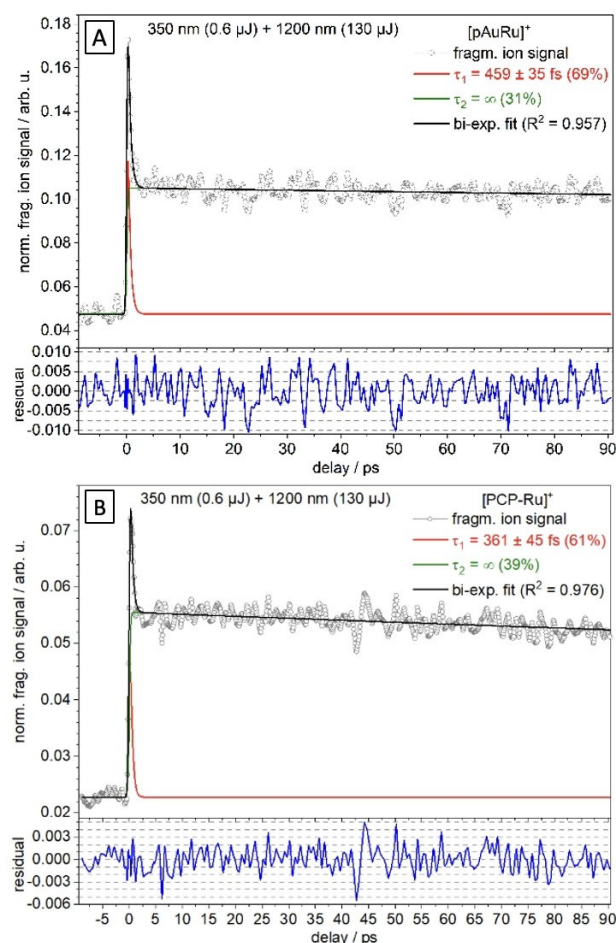
Figure 13. Normalized transient fragment ion intensity of [***p*AuRu**]$^+$ (**A**) and [**PCP-Ru**]$^+$ (**B**) recorded at λ_{pump} = 350 nm on a 100 ps time window; bi-exponential fit (black) is given along the fit decomposition (green and red). Fit residual is shown below (blue).

long-lived state with a lifetime τ$_2$ > 1 ns, likely a ^{3}MLCT state. Unfortunately, we cannot conclude on any influence or electronic coupling originating in the PPh$_2$AuCl substituent. Remarkably though, the comparison to the solution data above reveals that time constants in the intermediate range of a few ps to a few tens of ps (cf. τ$_2$ and τ$_3$ of Table 3) seem to be completely missing for the gas phase dynamics. A technical possibility, which we cannot completely exclude, is that these intermediate time constants might belong to states with a low probe amplitude and elude our τ-PD analysis technique. However, related complexes containing Ru-polypyridyl units have been successfully analyzed using τ-PD.[32,40]

To sum up, the τ-PD method was successfully applied to the isolated complexes [***p*AuRu**]$^+$ (**6**) and [**PCP-Ru**]$^+$ (**22**) resulting in intrinsic sub-ps formation of a long-lived electronically excited state. However, an influence of the PPh$_2$AuCl reactive center on the ultrafast dynamics was not detectable in the gas phase. In contrast, in solution, vibrational cooling or energy transfer to the solvent might be responsible for the richer dynamics and concomitant opening of different relaxation pathways.

Table 4. Catalytic application of the Au(I)/Ru(II) model complexes in a Meyer-Schuster rearrangement reaction.

entry	catalyst	yield [%][a]
1	PPh$_3$AuCl/Ru(bpy)$_3$Cl$_2$	73[b], 76[c]
2	PPh$_3$AuCl/Ru(bpy)$_2$(ppy)PF$_6$	73
3	**PCP-Au (21)/PCP-Ru (22)**	70
4	***p*AuRu (6)**	63
5	***m*AuRu (20)**	30
6	***o*AuRu (19)**	26
7	***gem*AuRu (18)**	13

23 (0.10 M, 156 µmol), **24** (624 µmol), **Au/Ru** or **AuRu** (3.90 µmol, 2.5 mol%), CH$_3$OH/CH$_3$CN (3:1), r.t., green LEDs (524 nm, 30 W), 12 h; [a] determined via ^{1}H NMR with 1,3,5-trimethoxybenzene as an internal standard; [b] isolated yield; [c] CH$_3$OH was used as a solvent.

Chemistry–A European Journal

Full Paper
doi.org/10.1002/chem.202102341

Chemistry
Europe
European Chemical
Societies Publishing

AuRu Heterobimetallic Cyclophanyl-Complexes in Meyer-Schuster Rearrangement: The Meyer-Schuster rearrangement (MSR) is a useful transformation of bifunctional, readily accessible propargyl alcohols into α,β-unsaturated carbonyl products.[41] Advancing the catalysis concept, Glorius,[38,42] Luna,[43] Shin,[44] and others have reported visible-light promoted arylative MSR as testing ground to explore dual catalytic pathways under Au(I) and Ru(II) catalysis. The mechanism for the arylative MSR was proposed by Glorius et al. and is based on previous reports on dual gold photoredox catalysis.[38] The catalytic cycle of the gold species is responsible for the formation of the arylated product. The ruthenium-based photoredox cycle oxidizes the intermediary Au(II) to Au(III) by single electron transfer. The MSR reaction was also reported by Shin and co-workers employing a 1:1 ratio of Au(I)/Ru(II) and were most fit for comparison with the heterobimetallic **AuRu** complexes. The diazonium salt **24** in combination with the propargylic alcohol **23** as test substrates afforded the arylated enone **25** in 76% yield (Table 4, entry 1) under the conditions reported by Shin and co-workers. To exclude possible electronic effects induced by the different coordination spheres that arise from the 2-phenylpyridine unit within the **AuRu** isomers, control experiments were also conducted following the literature procedure reported by Shin and co-workers using Ru-(bpy)$_2$(ppy)PF$_6$ as photocatalyst (Table 4, entry 2).

Furthermore, the impact of the PCP backbone on the overall reaction was investigated by applying the monometallic PCP derivatives **PCP-Au** (**21**) and **PCP-Ru** (**22**) (Table 4, entry 3). Demonstrating its potential as photoredox catalyst, **pAuRu** (**6**) performed the arylative MSR under irradiation with green LEDs (524 nm, 30 W) and afforded enone **25** in 63% yield (Table 4, entry 4). Employing the isomeric **AuRu** complexes **18–20** under similar reaction conditions led to a drop in yield. Reducing the M–M distance from **pAuRu** (**6**) to **mAuRu** (**20**) (entry 5) led to a reduction in yield, which decreased even further in case of **oAuRu** (**19**) and **gemAuRu** (**18**) (Table 4, entry 6 and 7). This reflects a structure-activity correlation and the observed reduction in yield by reducing the M–M distance supports electronic communication between the Au(I) and Ru(II) moiety which is likely to play a crucial role.

The oxidation potential **mAuRu** is the highest of the **AuRu** complexes, followed by **pAuRu**. In particular, the oxidation of the Ru(II) metal core to Ru(III) is more difficult for **mAuRu** and **pAuRu** by 0.15 V and 0.09 V, respectively when compared to the mononuclear **PCP-Ru** (**22**). That means that the oxidized form Ru(III) is less stable in **mAuRu** than in **PCP-Ru** (**22**). On the contrary, **gemAuRu** has almost the same oxidation potential as **PCP-Ru** (**22**), while **oAuRu** oxidation occurs 0.1 V earlier than in **PCP-Ru** (**22**). The presence of the electron-donating gold moiety stabilizes the Ru(III) core not only *via* a transannular effect, but also thanks to the close proximity of the two metal centers in **oAuRu**. Thanks to the position of the gold moiety, **oAuRu** and **gemAuRu** are more easily oxidized.

If we compare these results to the proposed mechanisms presented in the literature,[38] we can see that the first step, that is the oxidative quenching of Ru(II) by the aryl diazonium salt, should be easier for the **oAuRu**, followed by **gemAuRu**, **pAuRu**

and **mAuRu**. On the other hand, the second step, which is the reduction of Ru(III) by Au(II), is less favored for **mAuRu**. As the photocatalytic results for **oAuRu** and **mAuRu** are very similar to each other (26% and 30%, respectively), we can say that the redox potentials play an important role in the catalytic activity of these complexes but are not the only effect to be considered.

Conclusion

In summary, the formation of a series of cyclophanyl-derived Au(I)/Ru(II) decorated mono- and tunable heterobimetallic systems is described. Tailoring the cyclophanyl ligand by employing pseudo -*geminal*, -*ortho*, -*meta*, and -*para* substitution patterns, allow to precisely organize the **AuRu** metal centers in spatial orientation, and enable M–M distance modulation. The photophysical and electronic ground-state properties of the **AuRu** isomers were investigated and suggest M–M interactions. Exemplified for **pAuRu** (**6**), ultrafast transient absorption spectroscopy indicates dynamic and non-additive M–M interactions. Gas phase ultrafast photodissociation dynamics on isolated [**pAuRu**]$^+$ (**6**) confirms the intrinsic nature for the ultrafast formation of a long-lived electronically excited and reactive state.

At this point, a comprehensive interpretation of the ultrafast photo-induced dynamics is not yet possible – with **pAuRu** (**6**) being the only isomer investigated with fs time-resolved methods, so far. Hence, the impact of the current results of ultrafast transient spectroscopy on the photocatalytic mechanism is not clear, yet. The ongoing investigations of the other isomers including **mAuRu** (**20**), **oAuRu** (**19**) and **gemAuRu** (**18**) is necessary to get profound insights into the M–M interaction. The data of **pAuRu** (**6**) has shown a clear influence of the Au-moiety on the dynamics of **pAuRu** (**6**), when excited at 312 nm. In contrast, the excitation of **pAuRu** (**6**) at lower energy bands (405 or 495 nm) leads only to dynamics analogues to Ru-(bpy)$_2$(ppy). The wavelength-dependency of the photo-induced dynamics might as well affect the performance in photocatalysis. Thus, the preliminary results of the time resolved data are pointing at the benefits of further investigations on the system in catalysis, for example, considering photoreactivity under irradiation with different wavelengths.

As an initial study, the performance of the **AuRu** complexes proved viable in visible-light mediated arylative Meyer-Schuster rearrangement and emphasizes the viability of this approach. In this particular setup, the chemical reactivity is influenced by steric effects, electronic parameters, and a reduction in M–M distance between the Au(I) and Ru(II) moieties, which is likely to play a crucial role.

Developing catalysts by combining multiple metal centers is an emerging field of interest. The underlying mechanisms and influences that govern activity and selectivity in catalysts that combine multiple metal centers in a single molecule are scarcely understood. This is especially the case in light-driven reactions, where the different timescales for light absorption, generation of the excited state, and the actual chemical

reaction are crucial parameters. Concerning the net effects of changing metal to metal distance in complexes, more research represents an important step forward for its practical applications. With this work we hope to spark further investigations which will help in the design of enhanced catalysts.

Experimental Section

Deposition Numbers 2080313 (**3**), 2080314 (**11**), 2080315 (**21**), and 2080316 (**17**) contain the supplementary crystallographic data for this paper. These data are provided free of charge by the joint Cambridge Crystallographic Data Centre and Fachinformationszentrum Karlsruhe Access Structures service.

Experimental procedures and spectral data for all these new compounds are available in the Supporting Information.

Acknowledgments

Conflict of Interest

The authors declare no conflict of interest.

[1] a) J. Campos, *Nat. Chem. Rev.* **2020**, *4*, 696–702; b) J. A. Mata, F. E. Hahn, E. Peris, *Chem. Sci.* **2014**, *5*, 1723–1732; c) J. Park, S. Hong, *Chem. Soc. Rev.* **2012**, *41*, 6931–6943.

[2] a) S. Martínez, L. Veth, B. Lainer, P. Dydio, *ACS Catal.* **2021**, *11*, 3891–3915; b) I. Bratko, M. Gomez, *Dalton Trans.* **2013**, *42*, 10664–10681.

[3] a) R. Maity, B. S. Birenheide, F. Breher, B. Sarkar, *ChemCatChem* **2021**, *13*, 2337–237; b) K. L. Skubi, T. R. Blum, T. P. Yoon, *Chem. Rev.* **2016**, *116*, 10035–10074.

[4] I. G. Powers, C. Uyeda, *ACS Catal.* **2017**, *7*, 936–958.

[5] a) R. H. Duncan Lyngdoh, H. F. Schaefer, 3rd, R. B. King, *Chem. Rev.* **2018**, *118*, 11626–11706; b) P. C. Kamer, P. W. van Leeuwen, J. N. Reek, *Acc. Chem. Res.* **2001**, *34*, 895–904.

[6] Z. Hassan, S. Bräse, *Chem. Eur. J.* **2021**, https://doi.org/10.1002/chem.202102336.

[7] a) X. Lang, J. Zhao, X. Chen, *Chem. Soc. Rev.* **2016**, *45*, 3026–3038; b) M. Natali, S. Campagna, F. Scandola, *Chem. Soc. Rev.* **2014**, *43*, 4005–4018.

[8] a) Z. Hassan, E. Spuling, D. M. Knoll, J. Lahann, S. Bräse, *Chem. Soc. Rev.* **2018**, *47*, 6947–6963; b) G. J. Rowlands, *Isr. J. Chem.* **2012**, *52*, 60–75; c) S. E. Gibson, J. D. Knight, *Org. Biomol. Chem.* **2003**, *1*, 1256–1269; d) J. Paradies, *Synthesis* **2011**, 3749–3766; e) S. Bräse, M. Christmann, *Asymmetric Synthesis – The Essentials*, Wiley-VCH, Weinheim, **2006**.

[9] a) Z. Hassan, E. Spuling, D. M. Knoll, S. Bräse, *Angew. Chem. Int. Ed.* **2020**, *59*, 2156–2170; *Angew. Chem.* **2020**, *132*, 2176–2190; b) A. de Meijere, B. Stulgies, K. Albrecht, K. Rauch, H. A. Wegner, H. Hopf, L. T. Scott, L. Eshdat, I. Aprahamian, M. Rabinovitz, *Pure Appl. Chem.* **2006**, *78*, 813–830; c) O. R. P. David, *Tetrahedron* **2012**, *68*, 8977–8993; d) R. Gleiter, H. Hopf, *Modern Cyclophane Chemistry*, Wiley-VCH, Weinheim, **2004**; e) H. Hopf, *Isr. J. Chem.* **2012**, *52*, 18–19.

[10] S. F. Nelsen, A. E. Konradsson, J. P. Telo, *J. Am. Chem. Soc.* **2005**, *127*, 920–925.

[11] a) P. J. Pye, K. Rossen, R. A. Reamer, N. N. Tsou, R. P. Volante, P. J. Reider, *J. Am. Chem. Soc.* **1997**, *119*, 6207–6208; b) V. Rozenberg, T. Danilova, E. Sergeeva, E. Vorontsov, Z. Starikova, K. Lysenko, Y. Belokon, *Eur. J. Org. Chem.* **2000**, 3295–3303; c) J. F. Schneider, R. Fröhlich, J. Paradies, *Isr. J. Chem.* **2012**, *52*, 76–91; d) S. Ay, R. E. Ziegert, H. Zhang, M. Nieger, K. Rissanen, K. Fink, A. Kubas, R. M. Gschwind, S. Bräse, *J. Am. Chem. Soc.* **2010**, *132*, 12899–12905; e) S. Bräse, S. Dahmen, S. Hofener, F. Lauterwasser, M. Kreis, R. E. Ziegert, *Synlett* **2004**, *14*, 2647–2669, https://doi.org/10.1055/s-2004-836029; f) N. Hermanns, S. Dahmen, C. Bolm, S. Bräse, *Angew. Chem. Int. Ed.* **2002**, *41*, 3692–3694; *Angew. Chem.* **2002**, *114*, 3844–3846.

[12] C. Braun, M. Nieger, W. R. Thiel, S. Bräse, *Chem. Eur. J.* **2017**, *23*, 15474–15483.

[13] a) D. M. Knoll, T. B. Wiesner, S. M. Marschner, Z. Hassan, P. Weis, M. Kappes, M. Nieger, S. Bräse, *RSC Adv.* **2019**, *9*, 30541–30544; b) C. Schissler, E. K. Schneider, B. Felker, P. Weis, M. Nieger, M. M. Kappes, S. Bräse, *Chem. Eur. J.* **2021**, *27*, 3047–3054.

[14] a) P. Mücke, R. F. Winter, K. Kowalski, *J. Organomet. Chem.* **2013**, *735*, 10–14; b) P. Mücke, R. F. Winter, I. Novak, K. Kowalski, *J. Organomet. Chem.* **2012**, *717*, 14–22; c) P. Mücke, M. Zabel, R. Edge, D. Collison, S. Clément, S. Záliš, R. F. Winter, *J. Organomet. Chem.* **2011**, *696*, 3186–3197; d) S. Clement, T. Goudreault, D. Bellows, D. Fortin, L. Guyard, M. Knorr, P. D. Harvey, *Chem. Commun.* **2012**, *48*, 8640–8642; e) J.-L. Xia, W. Y. Man, X. Zhu, C. Zhang, G.-J. Jin, P. A. Schauer, M. A. Fox, J. Yin, G.-A. Yu, P. J. Low, S. H. Liu, *Organometallics* **2012**, *31*, 5321–5333.

[15] a) R. J. Felix, D. Weber, O. Gutierrez, D. J. Tantillo, M. R. Gagne, *Nat. Chem.* **2012**, *4*, 405–409; b) C. Sarcher, A. Lühl, F. C. Falk, S. Lebedkin, M. Kühn, C. Wang, J. Paradies, M. M. Kappes, W. Klopper, P. W. Roesky, *Eur. J. Inorg. Chem.* **2012**, *2012*, 5033–5042; c) F. C. Falk, R. Fröhlich, J. Paradies, *Chem. Commun.* **2011**, *47*, 11095–11097.

[16] a) C. Stephenson, T. Yoon, *Acc. Chem. Res.* **2016**, *49*, 2059–2060; b) M. Kozlowski, T. Yoon, *J. Org. Chem.* **2016**, *81*, 6895–6897; c) M. H. Shaw, J. Twilton, D. W. MacMillan, *J. Org. Chem.* **2016**, *81*, 6898–6926; d) A. B. Beeler, *Chem. Rev.* **2016**, *116*, 9629–9630; e) L. Marzo, S. K. Pagire, O. Reiser, B. Konig, *Angew. Chem. Int. Ed.* **2018**, *57*, 10034–10072; *Angew. Chem.* **2018**, *130*, 10188–10228; f) S. E. Braslavsky, *Pure Appl. Chem.* **2007**, *79*, 293–465; g) J. Busch, D. M. Knoll, C. Zippel, S. Bräse, C. Bizzarri, *Dalton Trans.* **2019**, *48*, 15338–15357.

[17] a) C. Bolm, K. Wenz, G. Raabe, *J. Organomet. Chem.* **2002**, *662*, 23–33; b) D. C. Braddock, I. D. MacGilp, B. G. Perry, *J. Org. Chem.* **2002**, *67*, 8679–8681; c) H. Hopf, L. Bondarenko, I. Dix, H. Hinrichs, *Synthesis* **2004**, *16*, 2751–2759, https://doi.org/10.1055/s-2004-834872; d) C. Braun, M. Nieger, W. R. Thiel, S. Bräse, *Chem. Eur. J.* **2017**, *23*, 15474–15483.

[18] a) D. M. Knoll, H. Šimek, Z. Hassan, S. Bräse, *Eur. J. Org. Chem.* **2019**, *36*, 6198–6202, https://doi.org/10.1002/ejoc.201901171; b) D. M. Knoll, C. Zippel, Z. Hassan, M. Nieger, P. Weis, M. M. Kappes, S. Bräse, *Dalton Trans.* **2019**, *48*, 17704–17708.

[19] J. Malberg, M. Bodensteiner, D. Paul, T. Wiegand, H. Eckert, R. Wolf, *Angew. Chem. Int. Ed.* **2014**, *53*, 2771–2775; *Angew. Chem.* **2014**, *126*, 2812–2816.

[20] a) B. Matt, C. Coudret, C. Viala, D. Jouvenot, F. Loiseau, G. Izzet, A. Proust, *Inorg. Chem.* **2011**, *50*, 7761–7768; b) P. G. Bomben, K. C. Robson, P. A. Sedach, C. P. Berlinguette, *Inorg. Chem.* **2009**, *48*, 9631–9643.

[21] S. Fernandez, M. Pfeffer, V. Ritleng, C. Sirlin, *Organometallics* **1999**, *18*, 2390–2394.

[22] a) N. V. Vorontsova, V. I. Rozenberg, E. V. Sergeeva, E. V. Vorontsov, Z. A. Starikova, K. A. Lyssenko, H. Hopf, *Chem. Eur. J.* **2008**, *14*, 4600–4617; b) D. C. Braddock, S. M. Ahmad, G. T. Douglas, *Tetrahedron Lett.* **2004**, *45*, 6583–6585; c) H. J. Reich, D. J. Cram, *J. Am. Chem. Soc.* **1969**, *91*, 3517–3526.

[23] C. Bolm, T. Focken, J. Rudolph, *Synthesis* **2005**, *3*, 429–436, https://doi.org/10.1055/s-2005-861800.

[24] S. V. Kruppa, F. Bäppler, C. Holzer, W. Klopper, R. Diller, C. Riehn, *J. Phys. Chem. Lett.* **2018**, *9*, 804–810.

[25] a) C. Larriba, C. J. Hogan, Jr., *J. Phys. Chem. A* **2013**, *117*, 3887–3901; b) C. Larriba, C. J. Hogan, *J. Comput. Phys.* **2013**, *251*, 344–363.

[26] V. Boekelheide, in *Cyclophanes I*, **1983**, 87–143.

[27] a) Y. Ohsawa, K. W. Hanck, M. K. DeArmond, *J. Electroanal. Chem. Interfacial Electrochem.* **1984**, *175*, 229–240; b) W. T. Kender, C. Turro, *J. Phys. Chem. A.* **2019**, *123*, 2650–2660.

[28] L. Buzzetti, G. E. M. Crisenza, P. Melchiorre, *Angew. Chem. Int. Ed.* **2019**, *58*, 3730–3747; *Angew. Chem.* **2019**, *131*, 3768–3786.

[29] R. Antoine, P. Dugourd, *Phys. Chem. Chem. Phys.* **2011**, *13*, 16494–16509.

[30] a) S. Xu, J. E. Smith, J. M. Weber, *Inorg. Chem.* **2016**, *55*, 11937–11943; b) M. Förstel, W. Schewe, O. Dopfer, *Angew. Chem. Int. Ed.* **2019**, *58*, 3356–3360; *Angew. Chem.* **2019**, *131*, 3394–3398; c) C. van der Linde, S. Hemmann, R. F. Hockendorf, O. P. Balaj, M. K. Beyer, *J. Phys. Chem. A* **2013**, *117*, 1011–1020; d) M. Srnec, R. Navratil, E. Andris, J. Jasik, J. Roithova, *Angew. Chem. Int. Ed.* **2018**, *57*, 17053–17057; *Angew. Chem.* **2018**, *130*, 17299–17303.

[31] F. Liedy, F. Bäppler, E. Waldt, Y. Nosenko, D. Imanbaew, A. Bhunia, M. Yadav, R. Diller, M. M. Kappes, P. W. Roesky, D. Schooss, C. Riehn, *ChemPhysChem* **2018**, *19*, 3050–3060.

[32] D. Imanbaew, J. Lang, M. F. Gelin, S. Kaufhold, M. G. Pfeffer, S. Rau, C. Riehn, *Angew. Chem. Int. Ed.* **2017**, *56*, 5471–5474; *Angew. Chem.* **2017**, *129*, 5563–5566.

[33] S. E. Greenough, G. M. Roberts, N. A. Smith, M. D. Horbury, R. G. McKinlay, J. M. Zurek, M. J. Paterson, P. J. Sadler, V. G. Stavros, *Phys. Chem. Chem. Phys.* **2014**, *16*, 19141–19155.

[34] T. Yanai, D. P. Tew, N. C. Handy, *Chem. Phys. Lett.* **2004**, *393*, 51–57.

[35] A. J. Bard, L. R. Faulkner, *Electrochemical methods: fundamentals and applications*, 2 ed., Wiley, New York, **2001**.

[36] a) S. H. Wadman, M. Lutz, D. M. Tooke, A. L. Spek, F. Hartl, R. W. Havenith, G. P. van Klink, G. van Koten, *Inorg. Chem.* **2009**, *48*, 1887–1900; b) W. W. Yang, Y. W. Zhong, S. Yoshikawa, J. Y. Shao, S. Masaoka, K. Sakai, J. Yao, M. A. Haga, *Inorg. Chem.* **2012**, *51*, 890–899; c) B. D. Koivisto, K. C. Robson, C. P. Berlinguette, *Inorg. Chem.* **2009**, *48*, 9644–9652; d) W.-W. Yang, L. Wang, Y.-W. Zhong, J. Yao, *Organometallics* **2011**, *30*, 2236–2240.

[37] a) T. Sato, K. Torizuka, R. Komaki, H. Atobe, *J. Chem. Soc. Perkin Trans. 2* **1980**, *4*, 561–568, https://doi.org/10.1039/P29800000561; b) T. Sato, K. Torizuka, *J. Chem. Soc. Perkin Trans. 2* **1978**, *11*, 1199–1204, https://doi.org/10.1039/P29780001199; c) S. Sankararaman, H. Hopf, I. Dix, Peter G. Jones, *Eur. J. Org. Chem.* **2000**, *15*, 2711–2716.

[38] A. Tlahuext-Aca, M. N. Hopkinson, R. A. Garza-Sanchez, F. Glorius, *Chem. Eur. J.* **2016**, *22*, 5909–5913.

[39] a) Q. Sun, B. Dereka, E. Vauthey, L. M. Lawson Daku, A. Hauser, *Chem. Sci.* **2017**, *8*, 223–230; b) Q. Sun, S. Mosquera-Vazquez, Y. Suffren, J. Hankache, N. Amstutz, L. M. Lawson Daku, E. Vauthey, A. Hauser, *Coord. Chem. Rev.* **2015**, *282–283*, 87–99; c) Q. Sun, S. Mosquera-Vazquez, L. M. Daku, L. Guenee, H. A. Goodwin, E. Vauthey, A. Hauser, *J. Am. Chem. Soc.* **2013**, *135*, 13660–13663.

[40] a) D. Imanbaew, Y. Nosenko, C. Kerner, K. Chevalier, F. Rupp, C. Riehn, W. R. Thiel, R. Diller, *Chem. Phys.* **2014**, *442*, 53–61.

[41] a) F. Justaud, A. Hachem, R. Grée, *Eur. J. Org. Chem.* **2021**, *4*, 514–542, https://doi.org/10.1002/ejoc.202001494; b) V. Cadierno, P. Crochet, S. E. Garcia-Garrido, J. Gimeno, *Dalton Trans.* **2010**, *39*, 4015–4031; c) D. A. Engel, G. B. Dudley, *Org. Biomol. Chem.* **2009**, *7*, 4149–4158; d) K. H. Meyer, K. Schuster, *Berichte der deutschen chemischen Gesellschaft (A and B Series)* **1922**, *55*, 815–819.

[42] M. N. Hopkinson, A. Tlahuext-Aca, F. Glorius, *Acc. Chem. Res.* **2016**, *49*, 2261–2272.

[43] B. Alcaide, P. Almendros, E. Busto, A. Luna, *Adv. Synth. Catal.* **2016**, *358*, 1526–1533.

[44] J. Um, H. Yun, S. Shin, *Org. Lett.* **2016**, *18*, 484–487.